TUNTWIN's Workshop

Session C: Scattering and diffraction techniques session

Funded by the Horizon 2020 Framework Programme of the European Union under the GA N° 952306

Session: Spectroscopy techniques

Synchrotron based X-ray Diffraction

Iris H.Valido

Synchrotron based X-ray diffraction

- Introduction
- Why use synchrotron radiation?
- Examples

Synchrotron based X-ray diffraction

- **Introduction**
- Why use synchrotron radiation?
- Examples

Synchrotron based X-ray diffraction: Introduction

What is diffraction?

X-rays scattered by a set atoms produce X-ray radiation in all directions, leading to interferences due to the coherent phase differences between the interatomic vectors that describe the relative position of atoms.

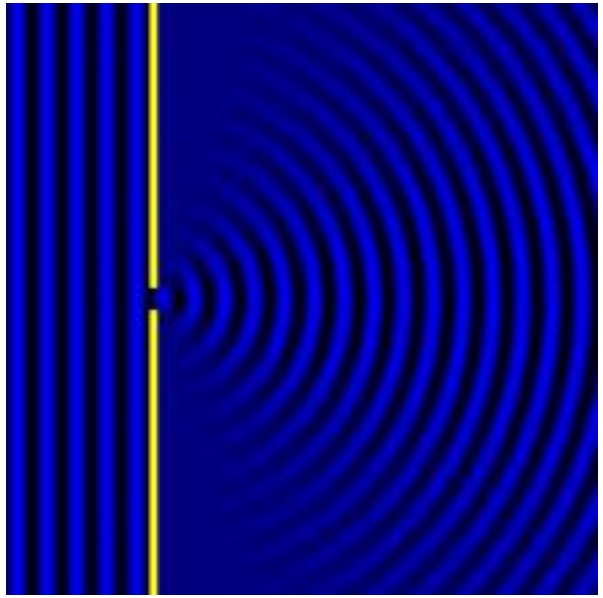

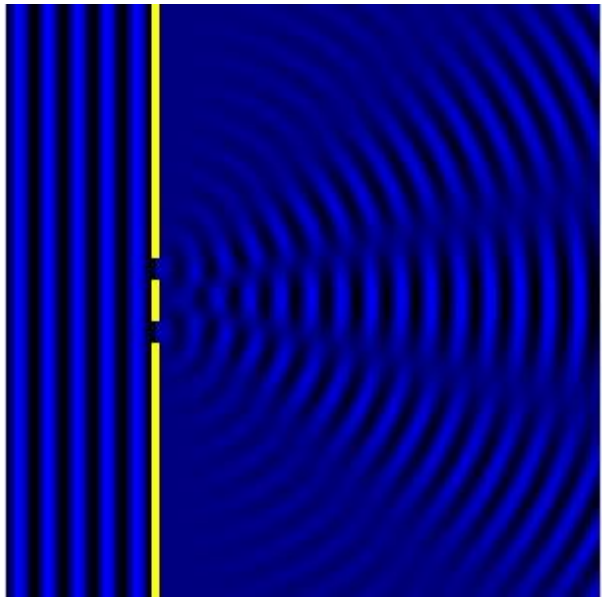

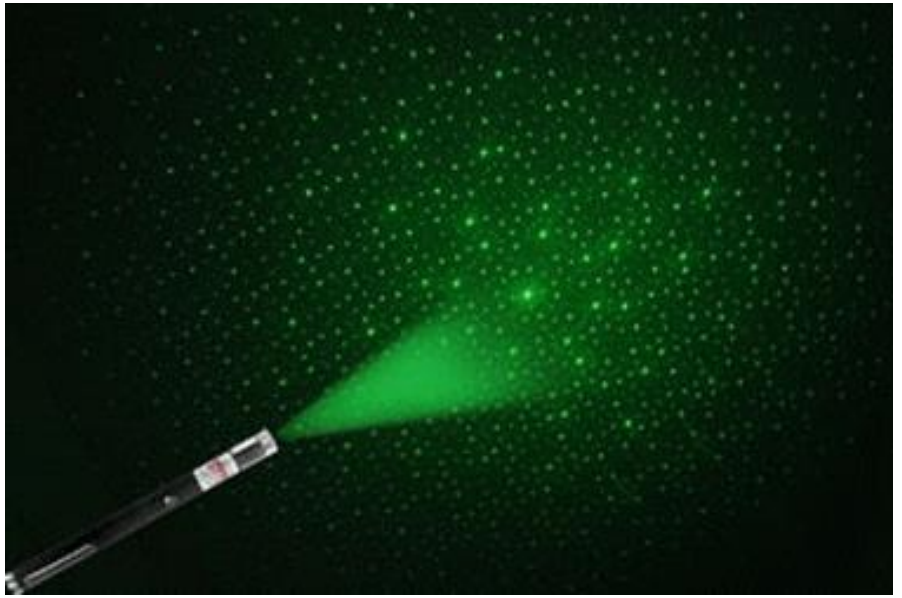

Bending of waves around the corners of an obstacle or through an aperture into the region of geometrical shadow of the obstacle/aperture

Synchrotron based X-ray diffraction: Introduction

How it works? Bragg's Law

"Crystals, at certain specific wavelengths and incident angles, produce intense peaks of reflected radiation (known as Bragg peaks)" W. L. Bragg

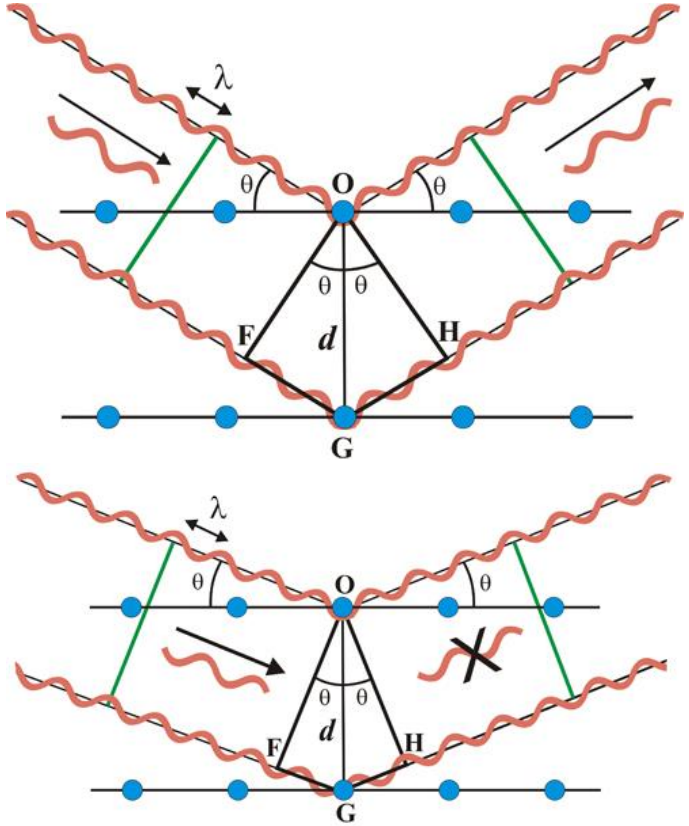

$$n\lambda = 2d \sin\theta$$

- 2θ = angle between incident and reflected beams
- d = spacing between planes
- λ = wavelength
- n = order of diffraction

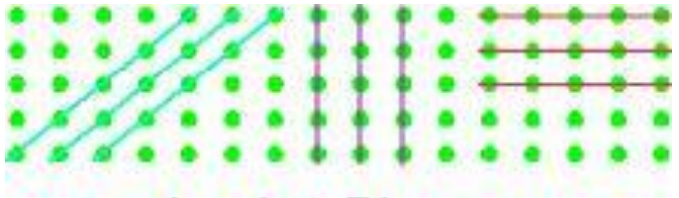

Lattice Planes

https://www.xtal.iqfr.csic.es/Cristalografia/parte_05_5-en.html

Synchrotron based X-ray diffraction: Introduction

How it works? Bragg's Law

Each Bragg reflection (hkl) is associated to a plane of atoms as described by crystallography.

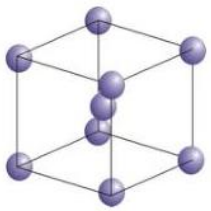

Body Centred Cubic

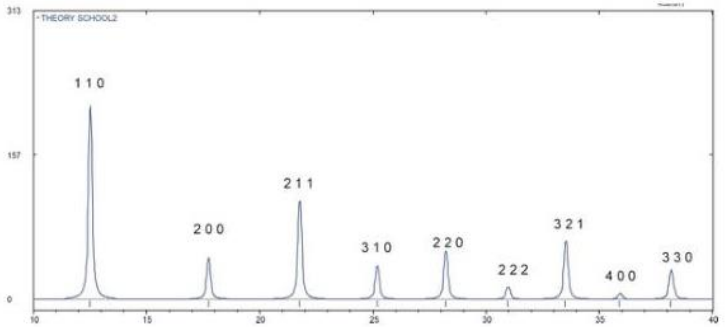

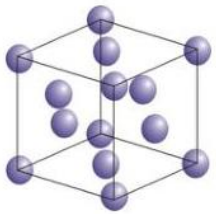

Face Centred Cubic

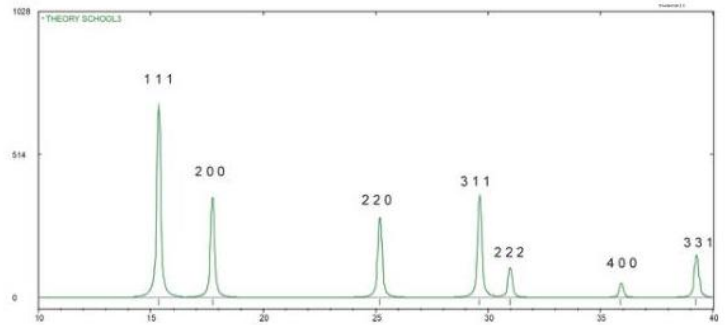

2θ

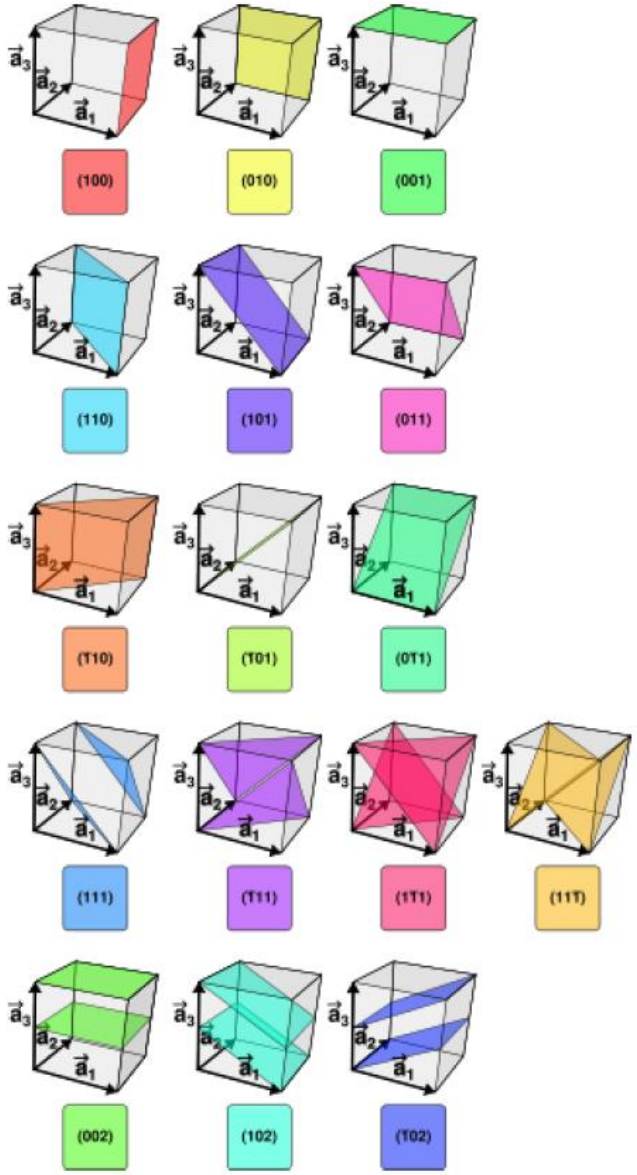

https://www.xtal.iqfr.csic.es/Cristalografia/parte_05_5-en.html

Synchrotron based X-ray diffraction: Introduction

Single crystal X-ray diffraction

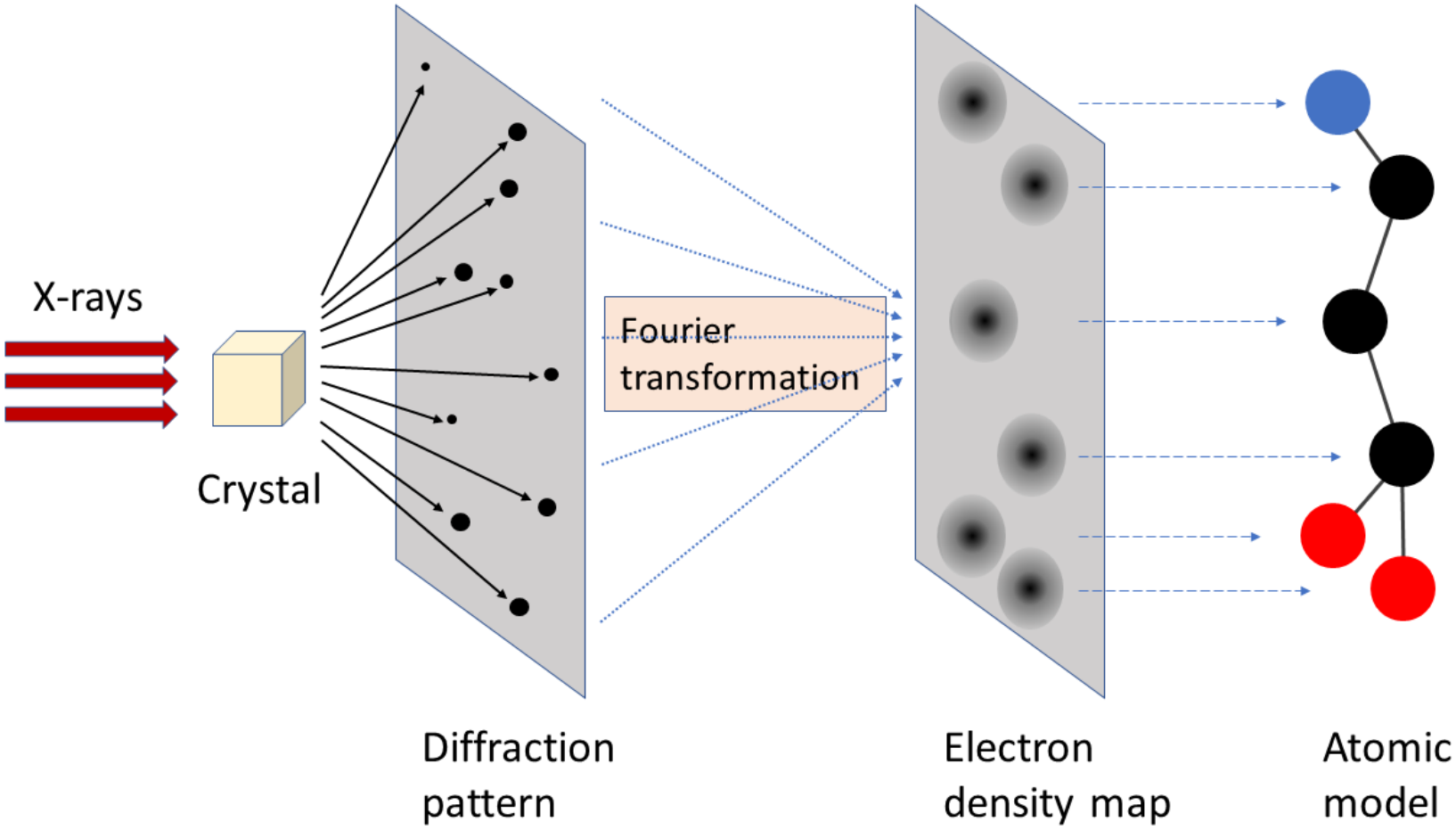

https://wiki.aalto.fi/pages/viewpage.action?pageId=119605795

Synchrotron based X-ray diffraction: Introduction

Powder X-ray diffraction

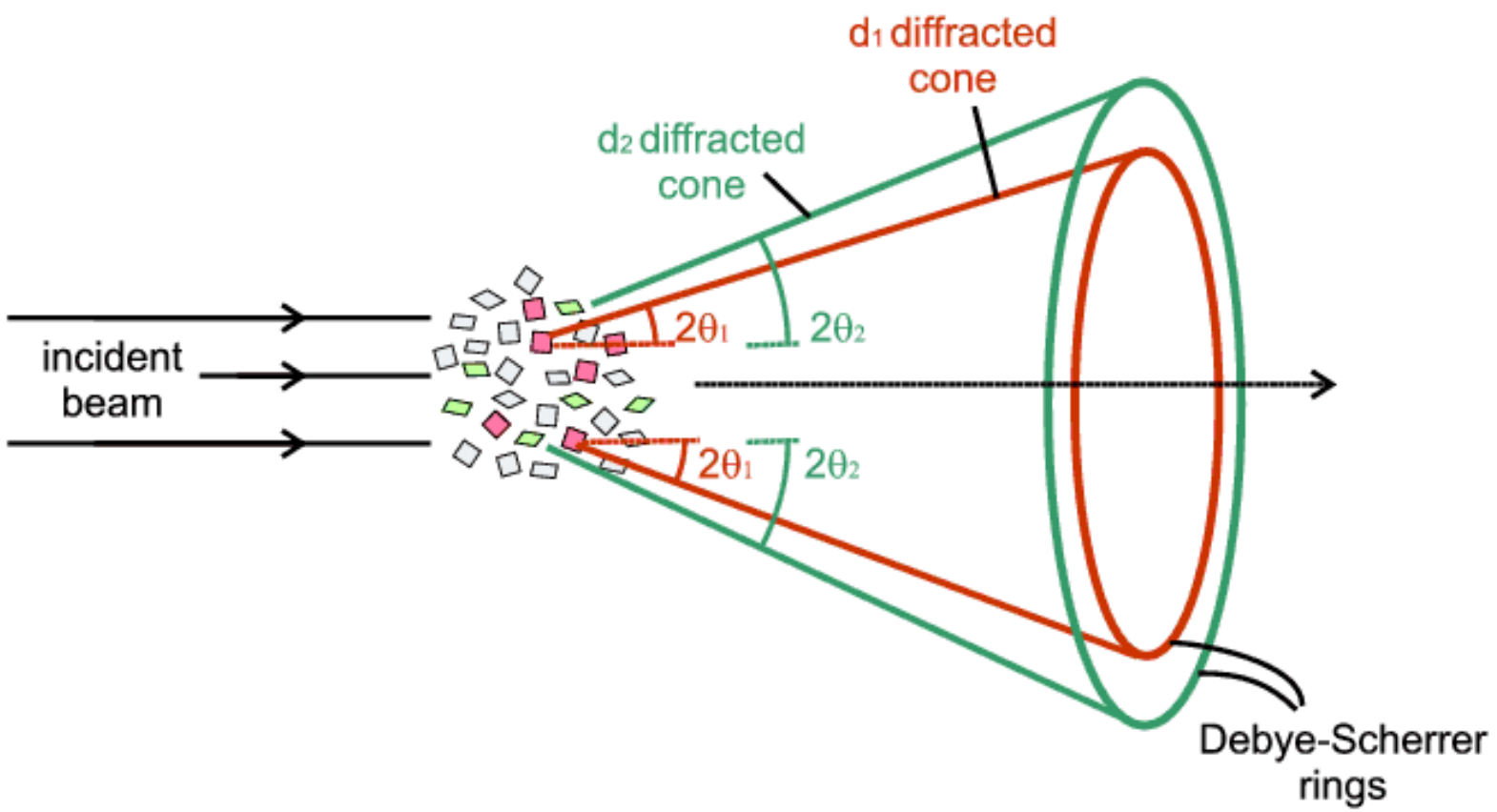

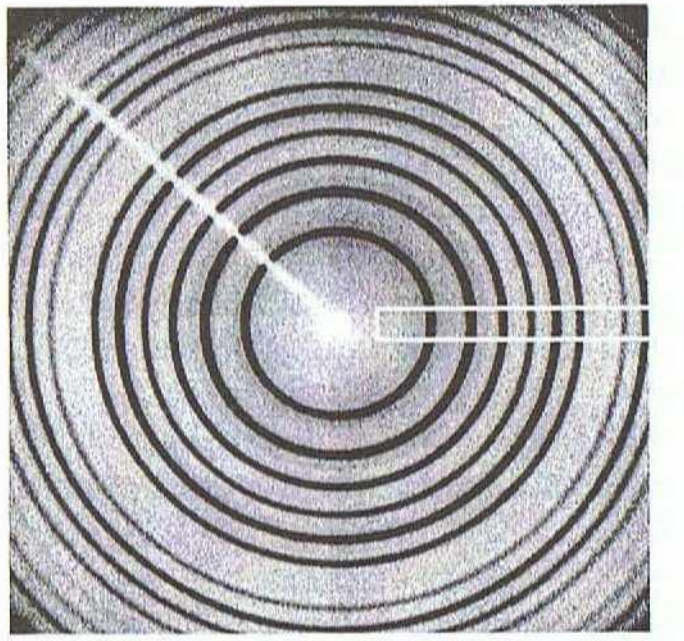

http://pd.chem.ucl.ac.uk/pdnn/diff2/kinemat2.htm

Synchrotron based X-ray diffraction: Introduction

Powder X-ray diffraction

- Peak position $2\theta_{hkl}$:
  - information on overall periodical arrangement of atoms
- Peak intensity I_{hkl}:
  - Type of atom in material
  - Position (x, y, z) of atoms in the structure (unit cell)
- Peak $FWHM_{hkl}$:
  - Microstructural features
    - Strains
    - Size
    - Stacking faults
    - …

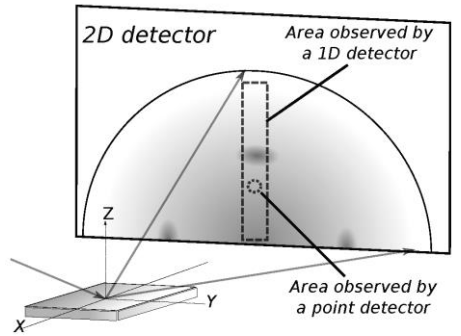

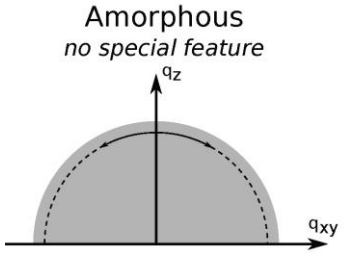

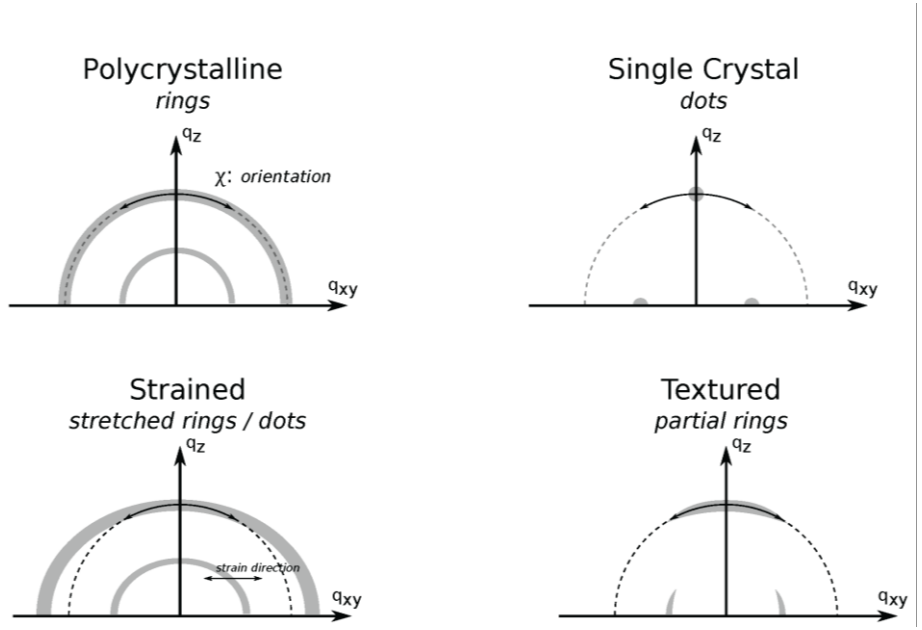

N. E. Widjomarko. Coatings 2016, 6(4), 54. doi.org/10.3390/coatings6040054

Synchrotron based X-ray diffraction: Introduction

Powder X-ray diffraction

Typical applications:

- Qualitative and quantitative phase analysis
- Structural analysis
- Stability and phase transitions
- Microstructure (crystalline size, microstrains)
- Microdiffraction

Synchrotron based X-ray diffraction

- Introduction
- **Why use synchrotron radiation?**
- Examples

Synchrotron based X-ray diffraction: Why use synchrotron?

Main Characteristics

- High intensity
- High monochromaticity
- Wavelength can be varied between experiments

Advantages

- High signal-to-noise ratio
- High angular resolution
- High speed of data collection

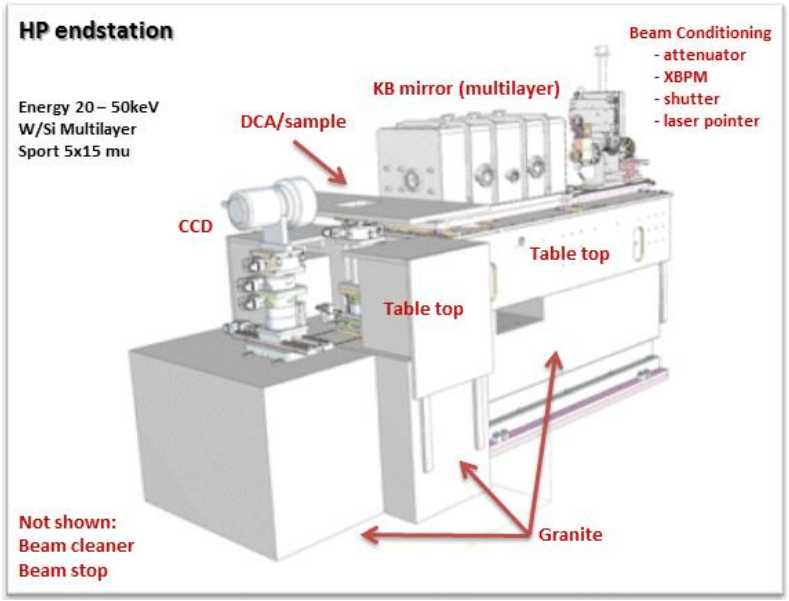

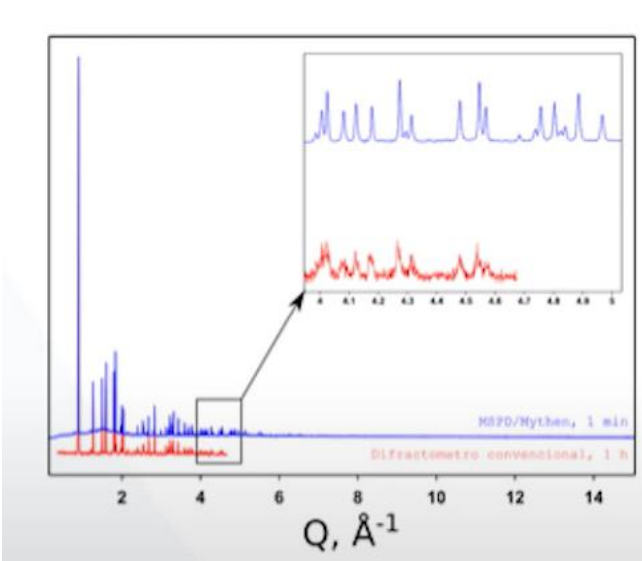

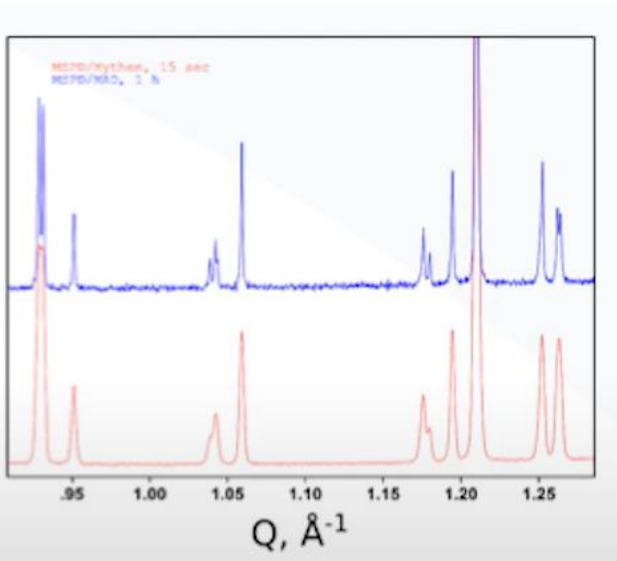

https://www.albasynchrotron.es/en/beamlines/bl04-mspd/information

Synchrotron based X-ray diffraction: Why use synchrotron?

Sample environments

- FMB Oxford hot air blower
- Oxford cryostream 700 series
- Dynaflow liquid He cryostat
- Capillary flow cell
- Equipment for the electrochemical studies
- On-line pressure calibration set-up (ruby lumiscence method)
- BETSA external ring heater
- External heating vacuum system
- IHE cryostat
- Navitar 12X online visualization system





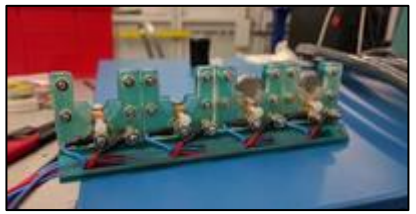

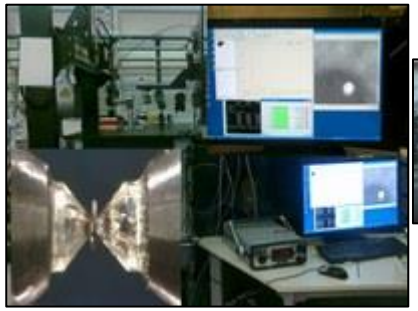


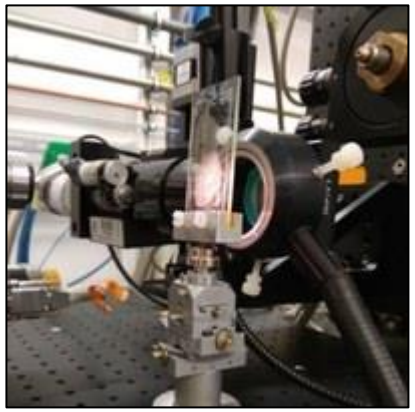
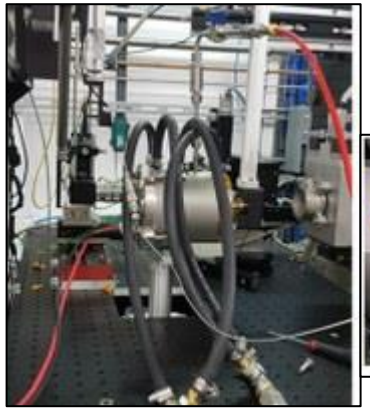


https://www.albasynchrotron.es/en/beamlines/bl04-mspd/sample-environments

Synchrotron based X-ray diffraction

- Introduction
- Why use synchrotron radiation?
- **Examples**

Synchrotron based X-ray diffraction: Examples

1. X-ray Total Scattering Study of Phases Formed from Cement Phases Carbonation

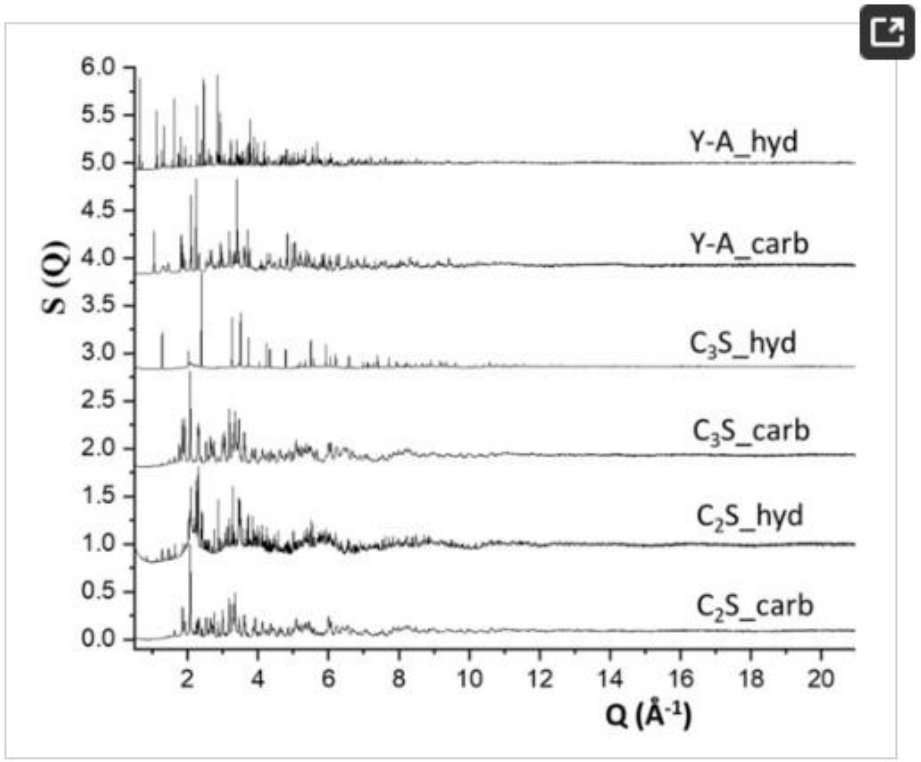

Figure 2. Synchrotron X-ray total scattering functions, S(Q), for the studied cement samples. The patterns were normalised with respect to their highest diffraction peaks and vertically displaced for adequate visualisation.

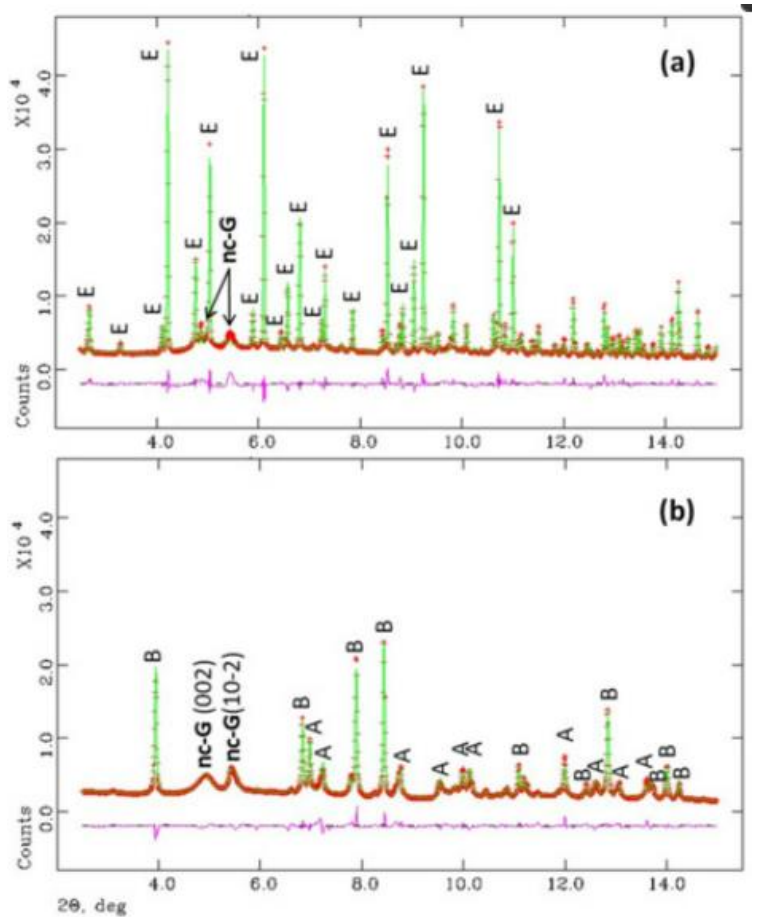

Figure 3. Selected low angle ranges (intensity vs 2θ) of the synchrotron Rietveld plots (λ = 0.41 Å) for (**a**) Y-A_hyd, hydrated for 1.5 months and (**b**) Y-A_carb paste after carbonation for 80 days at 3% of CO_2 (T = 20 °C and RH = 65%). The top pattern contains crystalline ettringite and very broad diffraction peaks of nano-gibbsite. The main peaks are labelled. Top pattern: ettringite (E) and nanocrystalline-gibbsite (**nc-G**). Bottom pattern: aragonite (A), bassanite (B), nanocrystalline-gibbsite (**nc-G**) [including their (hkl) indexes].

A. Cuestas, et al. Minerals 2021, 11(5), 519; doi.org/10.3390/min11050519

Synchrotron based X-ray diffraction: Examples

2. Operando Synchrotron X-ray Diffraction in Calcium Batteries: Insights into the Redox Activity of 1D Ca_3CoMO_6 (M = Co and Mn)

Figure 3. Sample holder with four coin cells to be simultaneously monitored *operando*, single coin-cell image, and an exploded view of a coin cell.

A. P. Black, et al. Energy Fuels 2021, 35, 13, 10898–10907. doi.org/10.1021/acs.energyfuels.1c01343

Synchrotron based X-ray diffraction: Examples

2. Operando Synchrotron X-ray Diffraction in Calcium Batteries: Insights into the Redox Activity of 1D Ca_3CoMO_6 (M = Co and Mn)

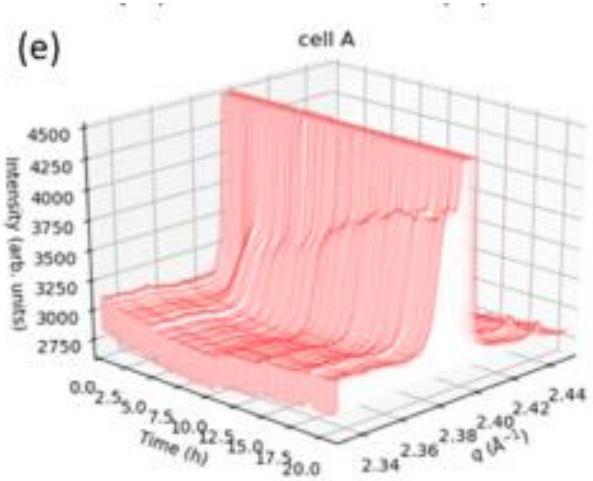

Figure 4. Potential vs capacity profiles from GCPL experiments on $Ca_3Co_2O_6$//AC cells using $Ca(BF_4)_2$ in EC/PC as the electrolyte at RT and C/50 rate (a), corresponding SXRD patterns (b) and zoom-in images (c,d), selected patterns correspond to the first and last pattern of cell (A) in black and light red, last oxidation and last reduction of cell (B) in red and dark green, and last ex situ pattern cell (B) in blue. (e,f) Zoom-in images of reflections 100 and 300 of in situ SXRD patterns of cells (A,B), respectively.

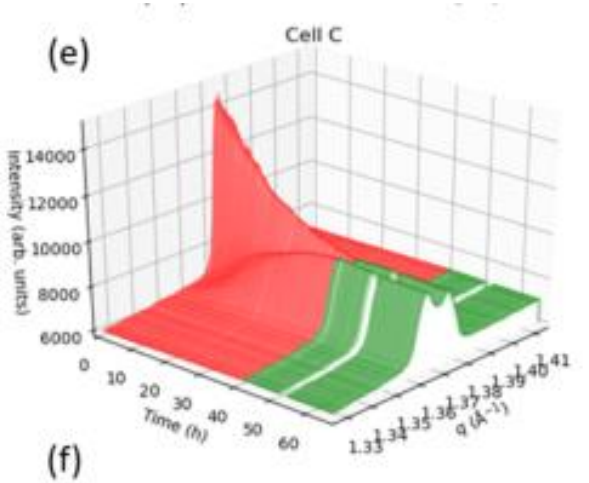

Figure 5. Potential vs capacity profiles from GCPL experiments on Ca_3CoMnO_6//AC cells using $Ca(BF_4)_2$ in EC/PC as the electrolyte at RT and C/50 (a), corresponding SXRD patterns (b) and zoom-in images (c,d), selected patterns correspond to pristine and last pattern in oxidation in black and red, last reduction in dark green, and last ex situ pattern of cell (C) in blue. (e,f) Zoom-in images of reflections 100 and 300 of in situ SXRD patterns, respectively.

A. P. Black, et al. Energy Fuels 2021, 35, 13, 10898–10907. doi.org/10.1021/acs.energyfuels.1c01343

Synchrotron based X-ray diffraction: Examples

3. Structural evolution, optical gap and thermoelectric properties of $CH_3NH_3SnBr_3$ hybrid perovskite, prepared by mechanochemistry

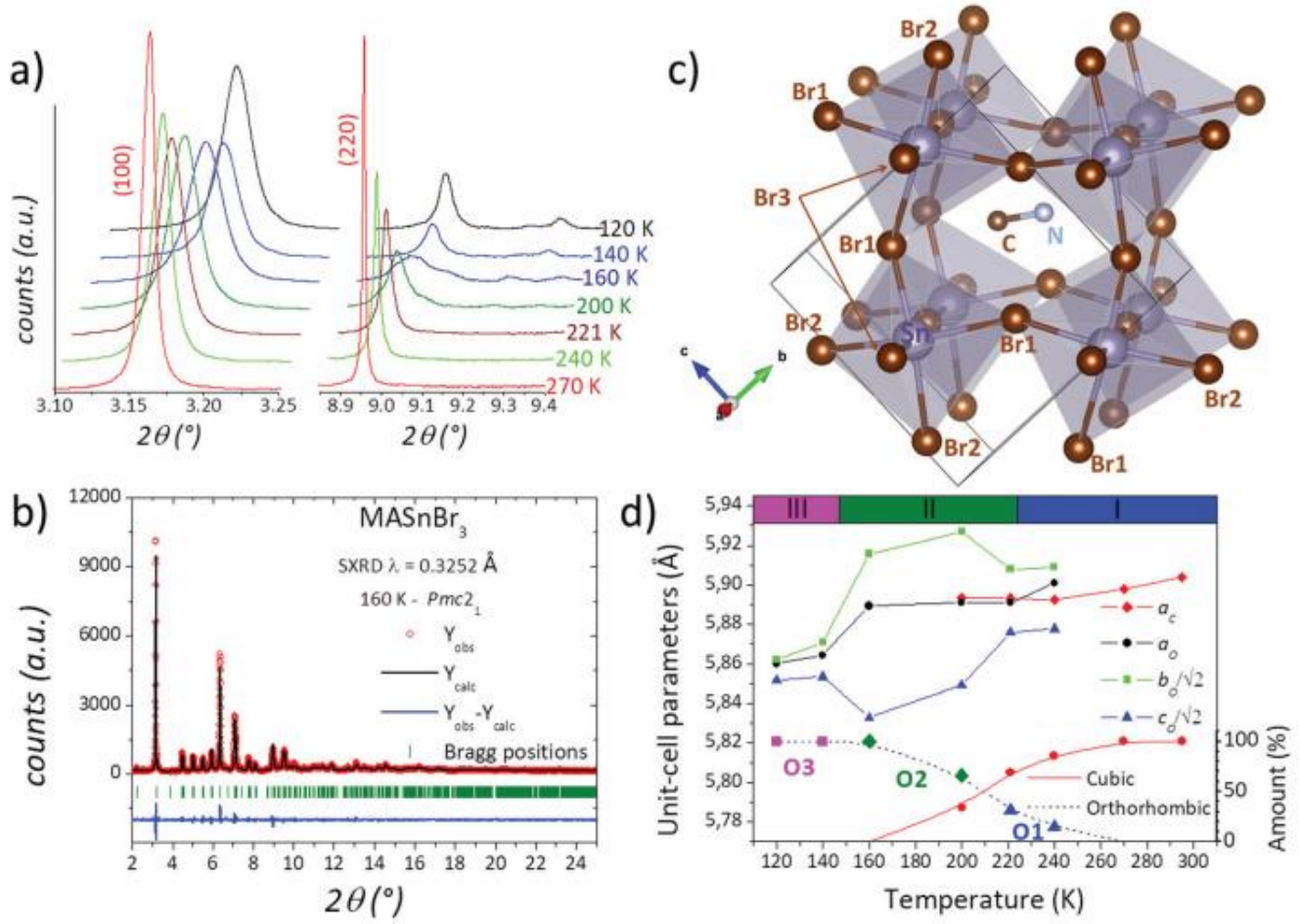

Fig. 2 (a) Thermal evolution of the (100) and (220) cubic lines from synchrotron diffraction. (b) Observed (circles), calculated (full line) and difference (bottom) Rietveld profiles for $MASnBr_3$ for SXRD data at 160 K. (c) Final crystal structure after Rietveld refinement at 160 K. (d) Evolution of the unit-cell parameters at different temperatures. The upper colour bars correspond to the calorimetric regions I, II and III.

C. A. Lopez, et al. Mater. Adv., 2021, 2, 3620. DOI: 10.1039/d1ma00196e

Synchrotron based X-ray diffraction: Examples

4. Determination of the Crystal Structures in the A-Site-Ordered $YBaMn_2O_6$ Perovskite

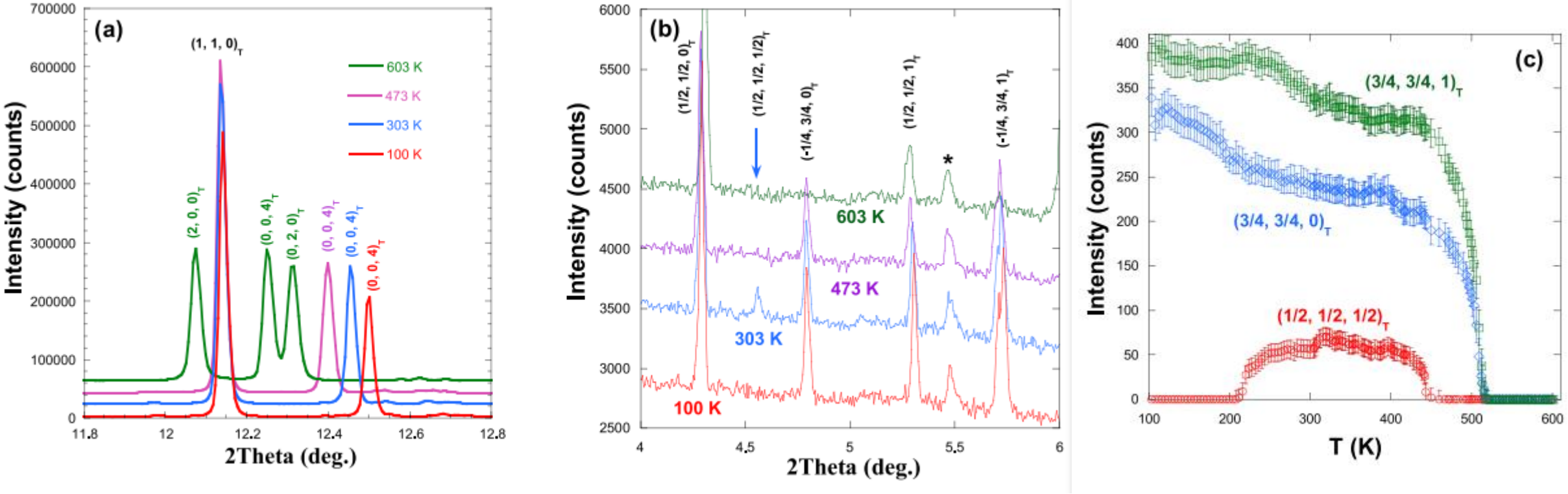

Figure 2. Details of the SXRPD patterns showing (a) the changes of the splitting in main diffraction peaks, indicating a unit cell change, and (b) the occurrence of different superstructure peaks at different temperatures. The asterisk marks the main peak of the secondary phase Y_2O_3 (0.3% in weight). (c) Temperature dependence of selected superstructure peaks. The subscript T in all panels indicates that indexation of the peaks is related to the parent tetragonal cell.

J. Blasco, et al. J. Phys. Chem. C 2021, 125, 35, 19467–19480. doi.org/10.1021/acs.jpcc.1c04697

Synchrotron based X-ray diffraction: Examples

5. Crystal Structure of $BaCa(CO_3)_2$ Alstonite Carbonate and Its Phase Stability upon Compression

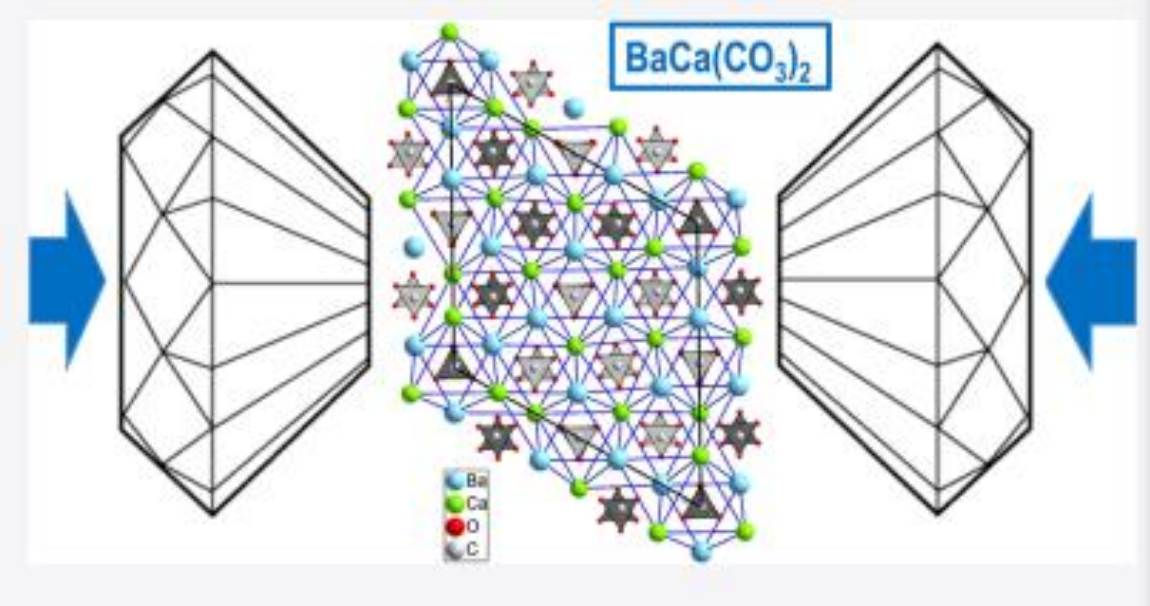

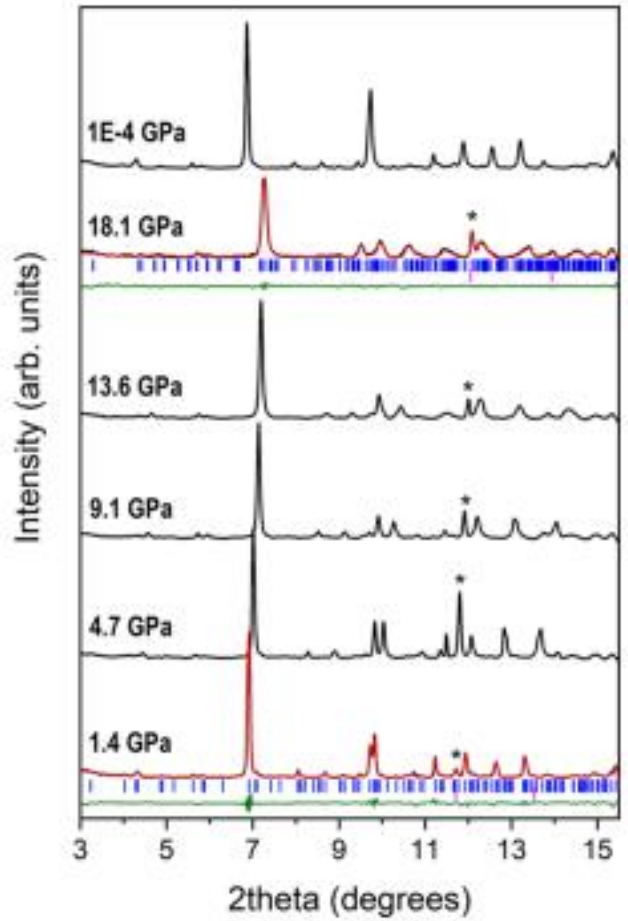

Figure 4. Powder XRD patterns of $BaCa(CO_3)_2$ alstonite at different pressures. The pattern of the recovered alstonite sample is shown on top. Asterisks denote the diffraction maxima of copper, the internal pressure gauge.

R. Chulia-Jordan, et al. ACS Earth Space Chem. 2021, 5, 5, 1130–1139. doi.org/10.1021/acsearthspacechem.1c00032

Synchrotron based X-ray diffraction: Examples

6. Unveiling the Structural Behavior under Pressure of Filled $M_{0.5}Co_4Sb_{12}$ (M = K, Sr, La, Ce, and Yb) Thermoelectric Skutterudites

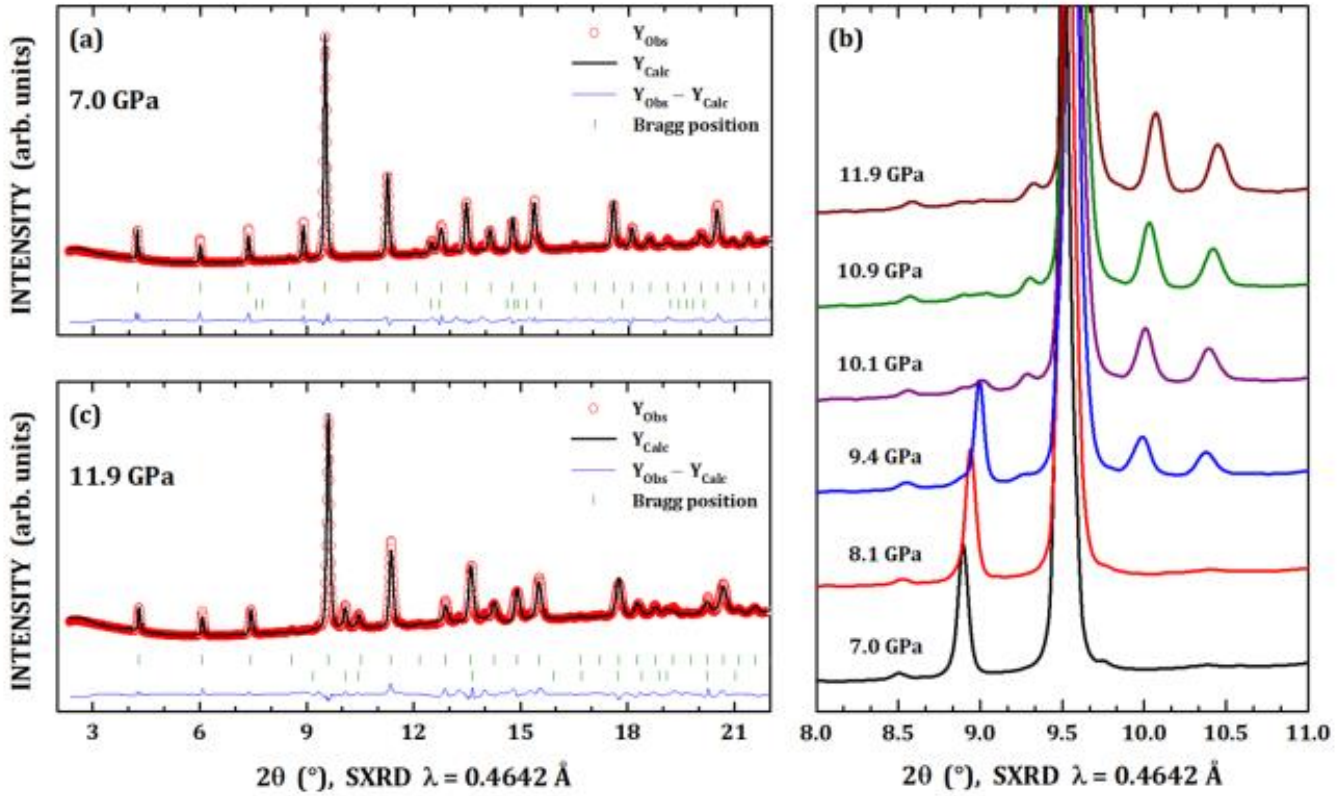

Figure 3. Synchrotron X-ray diffraction patterns of □Co_4Sb_{12} under 7.0 GPa (a) and 11.9 GPa (c). Details on the pressure evolution of Sb metal secondary phase (b), showing its phase transition from a rhombohedral (S.G. $R\bar{3}m$) to close-packed hexagonal (S.G. $P6_3/mmc$) phase around 9.4 GPa.

J. E. F. S. Rodrigues, et al. Inorg. Chem. 2021, 60, 10, 7413–7421. doi.org/10.1021/acs.inorgchem.1c00682

Synchrotron based X-ray diffraction: Examples

7. Discriminating the origin of calcium oxalate monohydrate formation in kidney stones via synchrotron microdiffraction

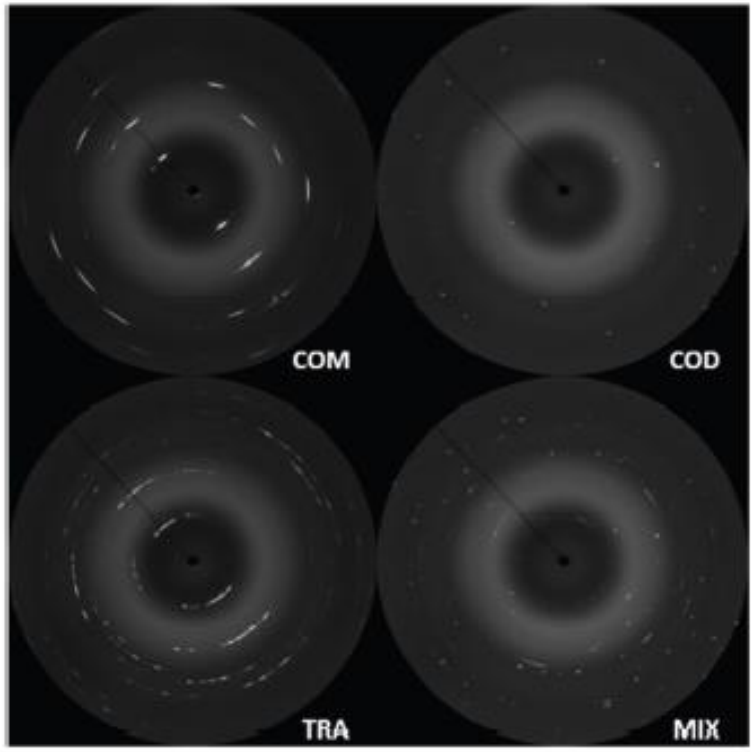

Fig. 4 2D-μXRD images of four representative points from calcium oxalate kidney stones, namely COM (top-left), COD (top-right), TRA (bottom-left) and MIX (bottom-right).

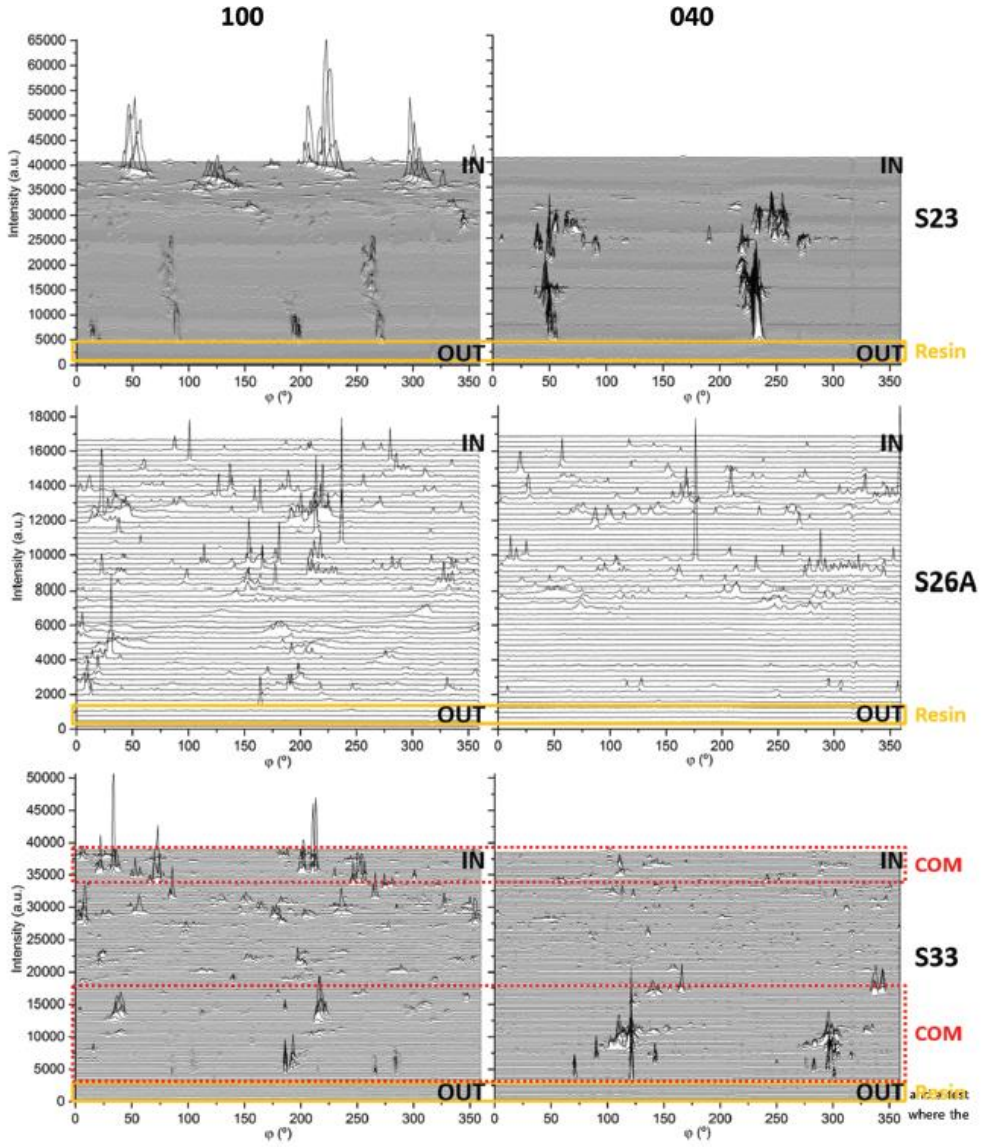

Fig. 5 Representation of the azimuthal plots for three samples, one representative of COM (top, S23), one representative of TRA (middle, S26A) and a test sample (bottom, S33), at reflections 100 and 040, left and right panels, respectively. The orange square (bottom of each plot) represents the resin where the stones are embedded, and the red dotted lines represent the two regions characterized as COM. The separation between points is 300 a.u. on the y-axis.

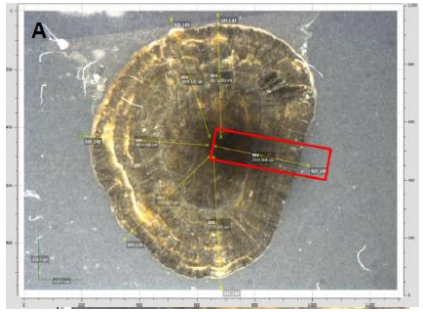

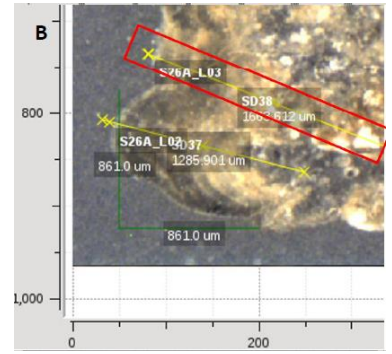

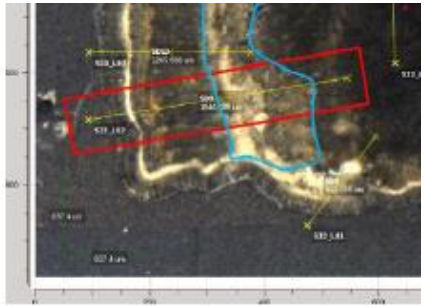

I. H.Valido, et al. Analyst, 2022, 147, 349. 10.1039/d1an01703a

Synchrotron based X-ray diffraction: Examples

8. Synchrotron X-ray microdiffraction to study dental structures in Cretaceous crocodylomorphs

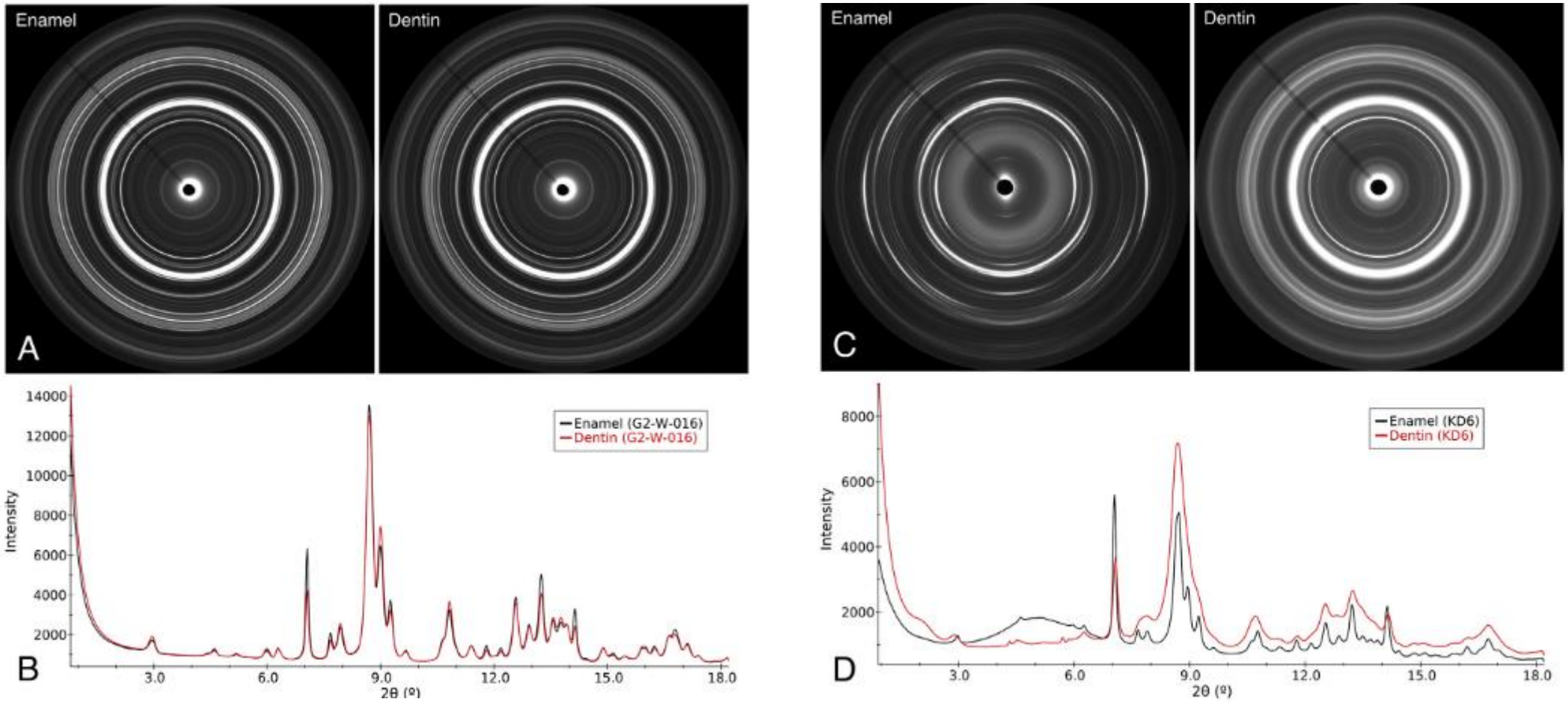

Fig. 3. Two-dimensional X-ray Diffraction (2D-XRD) patterns of the fossil tooth G2-W-016 (A), in the enamel (left) and the dentine (right). The enamel point is located at 70 μm and the dentine at 200 μm from the surface. Powder diffraction patterns obtained from the 2D-XRD data of the same tooth (B). 2D-XRD patterns of the modern tooth KD6 (C), in the enamel (left) and the dentine (right). The enamel point is located at 120 μm and the dentine at 600 μm from the surface. Powder diffraction patterns obtained from the 2D-XRD data of the same tooth (D).

O. Vallcorba, et al. Cretaceous Research 128 (2021) 104960. doi.org/10.1016/j.cretres.2021.104960

Synchrotron based X-ray diffraction: Examples

8. Synchrotron X-ray microdiffraction to study dental structures in Cretaceous crocodylomorphs

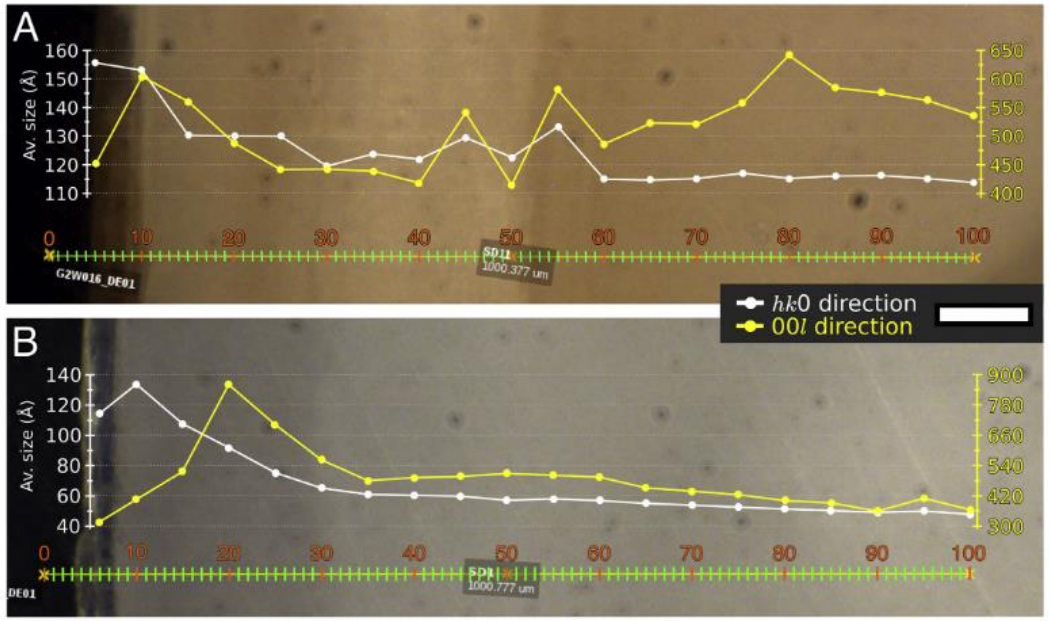

Fig. 4. Evolution of the hydroxyapatite average crystallite size in the *a*/*b* (*hk*0) and *c* (00*l*) directions with the teeth depth, for the fossil G2-W-016 (A) and the modern KD6 (B) teeth. Av: Average. Scale bar = 100 μm.

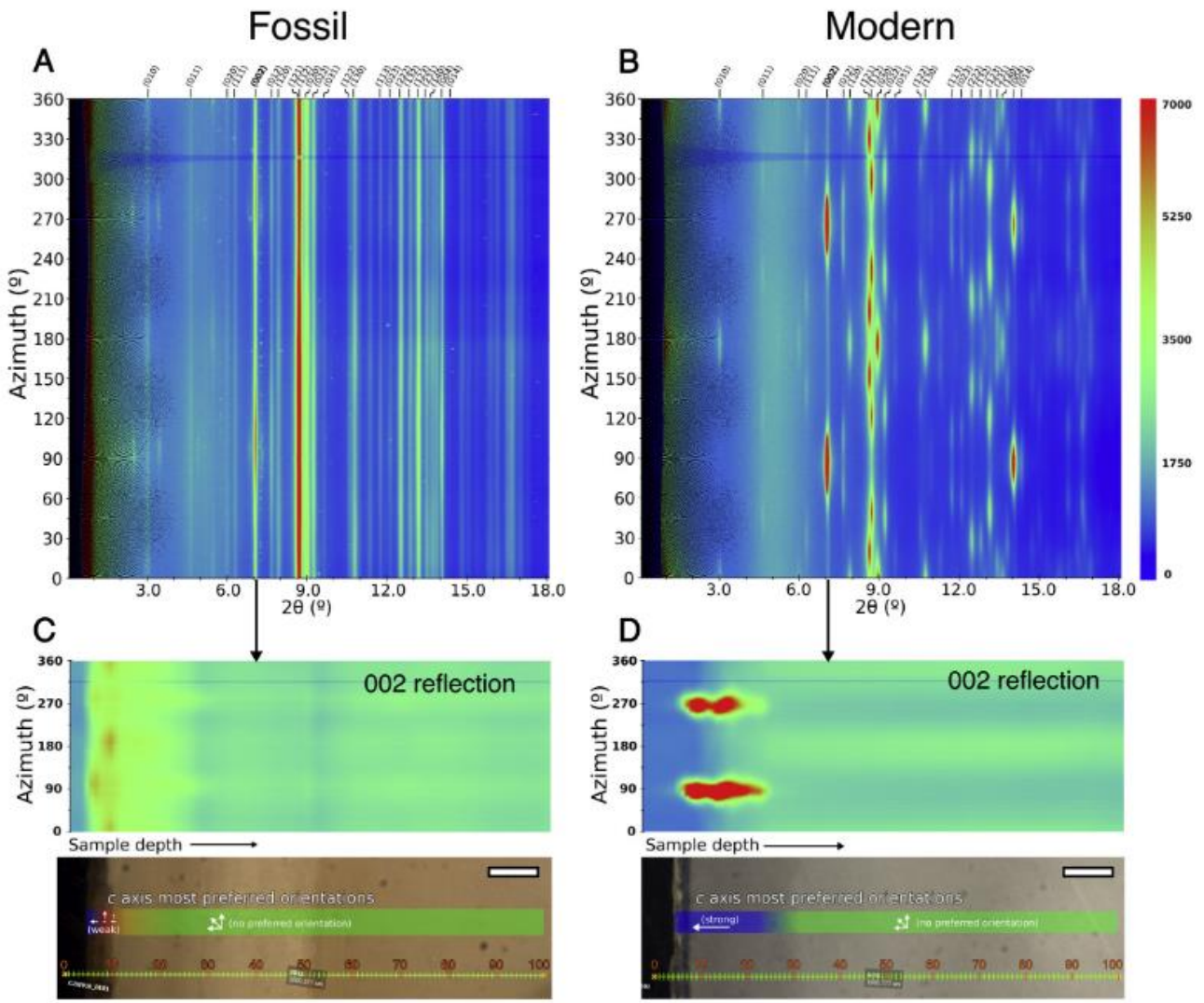

Fig. 5. Azimuthal plots from two-dimensional X-ray Diffraction (2D-XRD) for a single enamel point of the fossil G2-W-016 (A) and the modern KD6 (B) teeth. The hkl indices of the reflections are written on the top of each plot and the colour scale corresponds to the reflection intensities (detector counts). Stacking of azimuthal plots for the (002) reflection at each measured point of the same fossil (C) and modern (D) samples. Relative intensity at the same colour scale as the above plots. The preferred orientations of the c axis direction of the hydroxyapatite crystal structure for both teeth are represented on the respective images. Scale bar = 100 μm.

O. Vallcorba, et al. Cretaceous Research 128 (2021) 104960.
doi.org/10.1016/j.cretres.2021.104960

Synchrotron based X-ray diffraction: Examples

9. The color of the circus mosaic from Barcino (Roman Barcelona): Characterization, provenance and technology issues

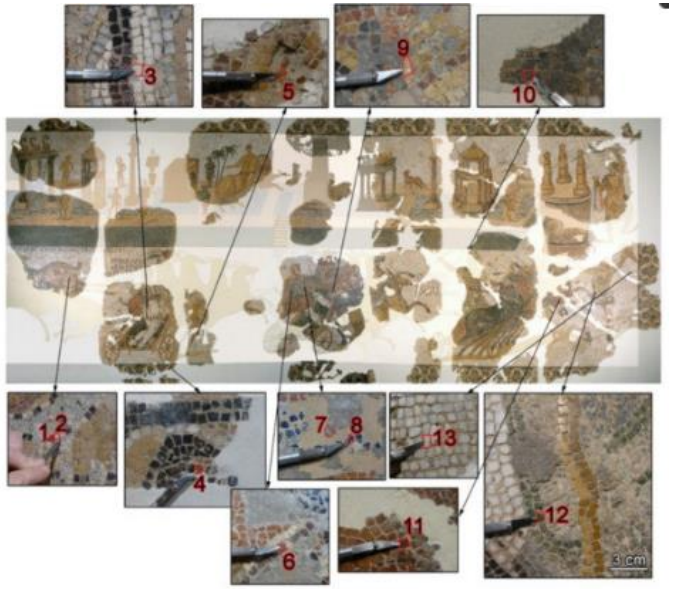

Figure 1. In the center, a general view of the Circus mosaic, and the smaller surrounding images illustrate the zoomed parts to identify the numbered tesserae in their original locations before their extraction.

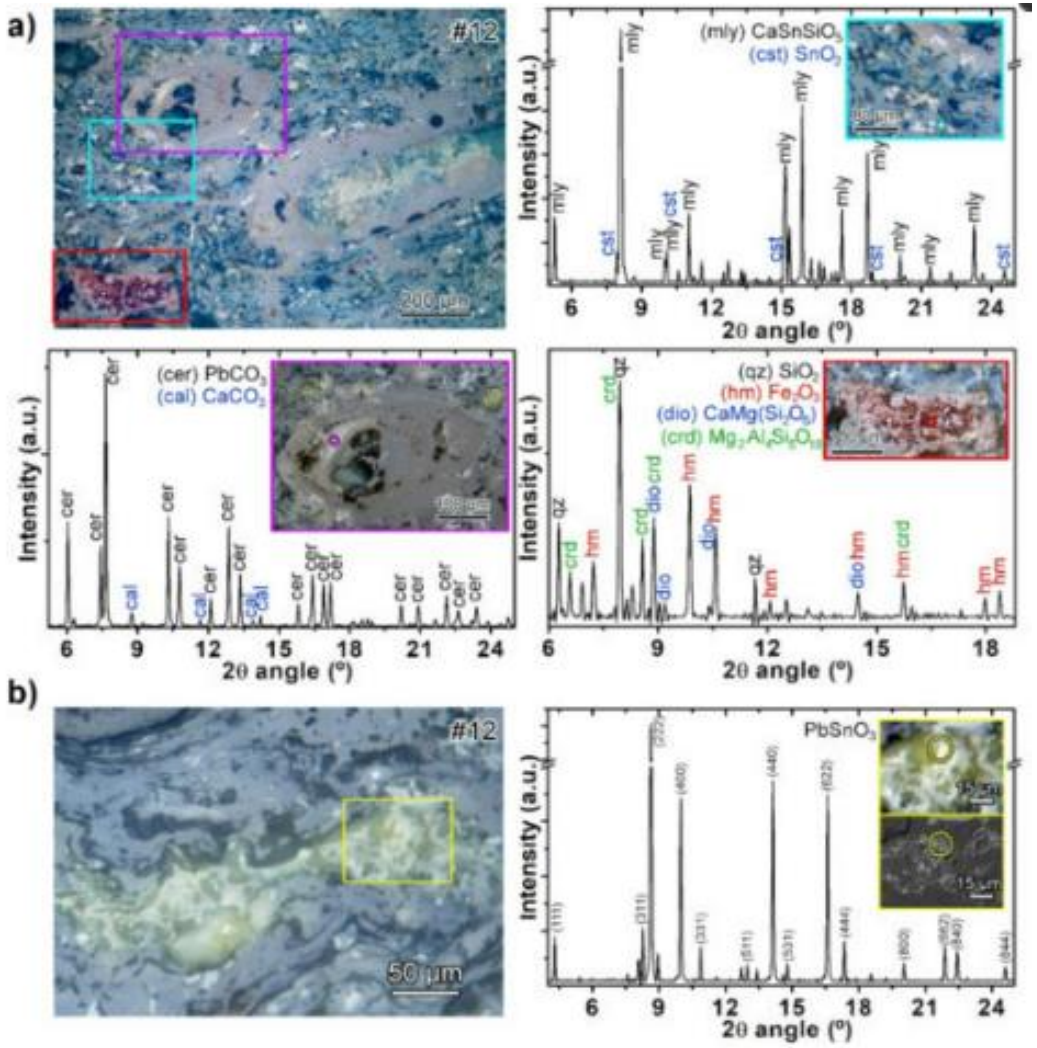

Figure 11. Representative diffractograms obtained by SR tts-µXRD from the crystalline features found within the green glass tessera #12: (**a**) POM image in RL mode with several highlighted colored rectangles, also shown as insets in the diffraction patterns, where the corresponding irradiated areas are marked with circles: ((**right**) grayish reflectance crystals including malayaite (mly) and cassiterite (cst), (**bottom-left**) pore filling including cerussite (cer) and calcite (cal); (**bottom-right**) reddish relict clod including quartz (qz), hematite (hm), diopside (dio) and cordierite (crd)). (**b**) POM image in RL mode with a highlighted rectangle, also shown as an inset (along with the equivalent SEM image) in the diffraction pattern on the right, where the corresponding irradiated area is marked with a circle, they correspond to yellowish reflectance crystals of cubic $PbSnO_3$.

L. Casas, et al. Minerals 2021, 11(7), 746; doi.org/10.3390/min11070746

TUNTWIN's Workshop

شكرا

Merci!

Thank you!

¡Gracias!

CONTACT DETAILS:

Iris H.Valido

Postdoctoral Researcher

Chemistry Department, Science Faculty

Campus UAB, 08193, Bellaterra

Barcelona, Spain.

Email: iris.henriquez@uab.cat

Commission européenne

Funded by the Horizon 2020 Framework Programme of the European Union under the GA N° 952306

TUNTWIN